Investigating magmatic processes in the early Solar System using the Cl isotopic systematics of eucrites

Available online at www.sciencedirect.com

ScienceDirect

Geochimica et Cosmochimica Acta 266 (2019) 582–597

Geochimica et Cosmochimica Acta

www.elsevier.com/locate/gca

Investigating magmatic processes in the early Solar System using the Cl isotopic systematics of eucrites

T.J. Barrett [a,*], J.J. Barnes [a,b], M. Anand [a,c], I.A. Franchi [a], R.C. Greenwood [a] B.L.A. Charlier [a,d], X. Zhao [a], F. Moynier [e], M.M. Grady [a,c]

[a] School of Physical Sciences, The Open University, Walton Hall, Milton Keynes MK7 6AA, UK
[b] Astromaterials Research and Exploration Science, NASA Johnson Space Center, Houston, TX 77058, USA
[c] Department of Earth Sciences, Natural History Museum, London SW7 5BD, UK
[d] Victoria University of Wellington, Wellington 6140, New Zealand
[e] Institut de Physique du Globe de Paris, Sorbonne Paris Cité, Univeristé Paris Diderot, 75005 Paris, France

Received 22 February 2019; accepted in revised form 15 June 2019; available online 22 June 2019

Abstract

Generally, terrestrial rocks, martian and chondritic meteorites exhibit a relatively narrow range in bulk and apatite Cl isotope compositions, with δ^{37}Cl (per mil deviation from standard mean ocean chloride) values between −5.6 and +3.8‰. Lunar rocks, however, have more variable bulk and apatite δ^{37}Cl values, ranging from ~−4 to +40‰. As the Howardite-Eucrite-Diogenite (HED) meteorites represent the largest suite of crustal and sub-crustal rocks available from a differentiated basaltic asteroid (4 Vesta), studying them for their volatiles may provide insights into planetary differentiation processes during the earliest Solar System history.

Here the abundance and isotopic composition of Cl in apatite were determined for seven eucrites representing a broad range of textural and petrological characteristics. Apatite Cl abundances range from ~25 to 4900 ppm and the δ^{37}Cl values range from −3.98 to +39.2‰. Samples with lower apatite H_2O contents were typically also enriched in ^{37}Cl but no systematic correlation between δ^{37}Cl and δD values was observed across samples. Modelled Rayleigh fractionation and a strong positive correlation between bulk δ^{66}Zn and apatite δ^{37}Cl support the hypothesis that Cl degassed as metal chlorides from eucritic magmas, in a hydrogen-poor environment. In the case of lunar samples, it has been noted that δ^{37}Cl values of apatite positively correlate with bulk La/Yb ratio. Interestingly, most eucrites show a negative correlation with bulk La/Yb ratio. Recently, isotopically light Cl values have been suggested to record the primary solar nebular signature. If this is the case then 4 Vesta, which accreted rapidly and early in Solar System history, could also record this primary nebular signature corresponding to the lightest Cl values measured here. The significant variation in Cl isotope composition observed within the eucrites are likely related to degassing of metal chlorides.

Keywords: Eucrites; Apatite; Chlorine Isotopes; NanoSIMS

1. INTRODUCTION

Chlorine is an important element being incompatible in nearly all silicates, volatile with a 50% condensation temperature of 940 K (Lodders, 2003), and strongly hydrophilic (Sharp et al., 2010a). The Cl isotope composition of meteorites is given in the standard delta notation (per mil, ‰) format where:

$$\delta^{37}Cl = \left\{ \left(\frac{R_{sample}}{R_{SMOC}} \right) - 1 \right\} * 1000$$

* Corresponding author.
E-mail address: thomas.barrett@open.ac.uk (T.J. Barrett).

https://doi.org/10.1016/j.gca.2019.06.024
0016-7037/Published by Elsevier Ltd.

R is $^{37}Cl/^{35}Cl$ ratio and the reference used is SMOC (standard mean ocean chloride) with a $\delta^{37}Cl$ value of 0.0‰ (Kaufmann et al., 1984). The $\delta^{37}Cl$ value can provide useful information regarding the isotopic reservoirs of volatiles that were present in the early Solar System and any subsequent secondary processes that may have occurred on different parent bodies (e.g., Sharp et al., 2007, 2013b; Bellucci et al., 2017). There is a relatively narrow range in the Cl isotope compositions of terrestrial rocks, martian meteorites and chondritic meteorites ($\delta^{37}Cl \sim -5.6$ to +3.8‰ although one data point for a martian meteorite does reach +8.6‰) (Sharp et al., 2007, 2013b, 2016; Williams et al., 2016; Bellucci et al., 2017; Manzini et al., 2017; Hu et al., 2019), with eucrites ranging up to ~+12‰ (Roszjar et al., 2015; Sarafian et al., 2017b) and the lunar samples being a clear exception to this rule. Based on data that are currently available in the peer-reviewed literature, lunar samples display a significant range in Cl isotopic composition, especially lunar apatite (e.g. Barnes et al., 2016, 2019; Potts et al., 2018), which shows $\delta^{37}Cl$ values ranging from $\sim -4 \pm 2$‰, lighter than typical terrestrial values (0 ± 2‰, e.g. Sharp et al., 2007), to extremely fractionated values of $\sim +40 \pm 2.9$‰ (e.g. Sharp et al., 2010b; Boyce et al., 2015; Barnes et al., 2016; Potts et al., 2018).

The Howardite-Eucrite-Diogenite (HED) meteorites comprise the largest suite of crustal and sub-crustal rocks available from a differentiated basaltic asteroid (most probably 4 Vesta) (McCord et al., 1970; De Sanctis et al., 2012; McSween et al., 2013). The eucrites are also some of the oldest igneous rocks in the Solar System, typically with crystallisation ages from 4547 Ma to 4559 Ma (Misawa et al., 2005; Zhou et al., 2013; Touboul et al., 2015). Characterising the volatile inventories of eucrites is therefore central to understanding the processes that operated on asteroid parent bodies early in the Solar System history.

Based on their petrographic and chemical characteristics, eucrites are subdivided into basaltic and cumulate groups (Stolper, 1977; Mayne et al., 2009). The basaltic eucrites, the most numerous of all eucrites, are fine to medium-grained igneous rocks, and predominately composed of pigeonite and calcic plagioclase (ranging from bytownite to anorthite; Mittlefehldt, 2015). Cumulate eucrites are thought to be mixtures of cumulus minerals (pyroxene and plagioclase) and trapped melt whose parent magmas were similar to basaltic eucrites (Treiman, 1997; Barrat et al., 2000; Mittlefehldt and Lindstrom, 2003; Barrat, 2004). These cumulate eucrites potentially formed at greater depths where elevated temperatures kept some isotopic systems open for a significant period of time after eucrite formation (Bogard and Garrison, 2003).

The basaltic eucrites can be further subdivided based on their bulk-rock magnesium number (Mg#) or FeO_{total}/MgO weight ratio, and their Ti and incompatible trace element abundances (Stolper, 1977; Hsu and Crozaz, 1996; Hutchison, 2004; Barrat et al., 2007) into the Main Group-Nuevo Laredo (hereafter referred to as Main Group) and Stannern trends. The Main Group comprises the majority of the basaltic eucrites and is widely accepted as a fractional crystallisation trend (Stolper, 1977; Warren and Jerde, 1987; Mittlefehldt and Lindstrom, 2003) showing a linked increase in incompatible element abundance with decreasing Mg#. The Stannern trend eucrites have very similar major element abundances to Main Group eucrites but have higher abundances of Ti and incompatible elements, enrichments that are not linked to Mg# (Barrat et al., 2000; Hutchison, 2004; Barrat et al., 2007), they also have isotopically heavier Fe isotopic compositions than other eucrites (Wang et al., 2012). Barrat et al. (2007) suggested that the contamination of Main Group eucrites by crustal melts could explain both the elevated incompatible element concentrations and the distinctive Eu, Sr, and Be anomalies shown by Stannern trend eucrites. A partial melt would leave behind a residual eucrite with LREE depletion, which Yamaguchi et al. (2009) observed in several eucrites and believed to be a third geochemical trend dubbed the 'residual eucrites'.

Apatite [$Ca_5(PO_4)_3$(F, Cl, OH)] is a widely distributed accessory phase in planetary materials (e.g. Delaney et al., 1984; Sarafian et al., 2013; McCubbin and Jones, 2015) and was the only known volatile-bearing mineral phase in eucrites until preliminary studies by Stephant et al. (2016) and Sarafian et al. (2017c) measured the H_2O abundance and H isotopic composition of eucritic pyroxenes (up to 193 ± 11 ppm H_2O). Apatite contains hydrogen in the form of structurally bound OH^-, but in this contribution the measured OH abundance is converted to its weight equivalent H_2O for the purposes of comparing the data with those in the literature. Currently, the data on volatiles (H and Cl) in apatite from eucrites is limited, owing to a small number of studies (Sarafian et al., 2013, 2014, 2017b; Roszjar et al., 2015; Barrett et al., 2016; Schneck et al., 2016). In order to investigate the history of volatiles in eucrites, the Cl isotopic composition of apatite from the cumulate eucrite Moore County and the basaltic eucrites Agoult, Dar al Gani (DaG) 844, DaG 945, Millbillillie, North West Africa (NWA) 2362 and Stannern were measured. Apatite grains in all samples except Agoult and NWA 2362 were previously analysed for their H isotopic composition and H_2O abundances (Barrett et al., 2016). The zinc isotopic composition of DaG 945 was also measured specifically to test the hypothesis of Cl isotope fractionation via metal chlorides which is outlined below in Section 5.2.

2. SAMPLE DESCRIPTIONS

The majority of samples studied here have been previously described in (Barrett et al., 2016) for the same thin sections and apatite grains. Sample descriptions for these meteorites are included in the supplementary material of this work; new residual eucrite samples are described in Yamaguchi et al. (2009) and also briefly in the supplementary material. Representative back-scattered electron (BSE) images illustrating the textural and petrological context of the apatite grains analysed in this study are provided in the supplementary material (Fig. SM1). See Table 1 for an overview of samples studied here.

Table 1
Main characteristics of the meteorites studied. WG = Weathering Grade, MG = Metamorphic Grade. Cosmic ray exposure (CRE) ages for eucrites Stannern and Millbillillie are taken from Miura et al. (1998) and Moore County age from Eugster and Michel (1995).

Meteorite	Find/Fall	Geochemical trend	Brecciation	WG	MG	CRE age (Ma)
Agoult	Find	Residual				
DaG 844	Find		Polymict	W3	6	
DaG 945	Find	Residual	Brecciated	W1	4	
Millbillillie	Fall	Main Group	Polymict		6	20
Moore County	Fall	Cumulate	Unbrecciated			7
NWA 2362	Find	Residual				
Stannern	Fall	Stannern Trend	Monomict		4	35

3. METHODS

3.1. Scanning electron microscopy

To locate appropriate apatite grains (i.e. large enough grains with sufficient crack-free areas for isotope analyses) each polished thin-section was carbon-coated using an EMITECH K950X Turbo carbon sputter coater and examined at The Open University using a Quanta 3D Focused-Ion-Beam Scanning Electron Microscope (FIB-SEM) fitted with an Oxford Instrument INCA energy dispersive X-ray detector. An electron beam with an acceleration voltage of 20 kV and a beam current of 0.6 nA was used for the acquisition of all the backscatter electron (BSE) images and elemental X-ray maps. Whole-section elemental X-ray maps were acquired for each sample and correlated hotspots of Ca and P X-rays were used to locate phosphates, which were subsequently investigated by rapid energy dispersive spectroscopy (exposure ~30 s) to distinguish between apatite and merrillite [$(Mg, Fe)_2REE_2Ca_{16}P_{14}O_{56}$]. Once located, high-resolution BSE and secondary electron (SE) images of the phosphates were collected to aid subsequent ion-probe work.

3.2. Nano Secondary Ion Mass Spectrometry (NanoSIMS) protocol

The Cl content and Cl isotopic compositions of apatite were measured using the Cameca NanoSIMS 50L at The Open University in multi-collection mode using a refined protocol based on Tartèse et al. (2014) and Barnes et al. (2016), acquiring negative secondary ions of ^{18}O, ^{35}Cl, ^{37}Cl, and $^{40}Ca^{19}F$, simultaneously on electron multipliers. Prior to ion-probe analyses, the carbon coat used for SEM analysis was removed, samples cleaned, and then coated with a ~30 nm gold coat. Samples were stored in a vacuum oven at ~55 °C for at least 24 hours prior to transfer to the NanoSIMS airlock. Once in the airlock, each sample was left to degas under vacuum at ~55 °C for at least another day before transferring it to the vessel chamber. The primary current for three of the four analytical sessions was ~50 pA (in Cs^+ mode). Counts per second (cps) for Cl in these sessions were also kept to below 85,000 using the aperture slit (AS) and entrance slit (ES) as experience has shown a significant increase in detector ageing at, and above this value. The January 2016 session used the lower probe current of ~25 pA without AS to avoid detector ageing owing to excessive counts on the electron multipliers. Mass $^{40}Ca^{19}F$ was monitored in real time imaging (RTI) mode to identify apatite grains prior to analyses. Typically, a 5 μm × 5 μm area was analysed, however for some smaller grains this area was decreased to as small as 3 μm × 3 μm. For samples analysed at smaller raster areas than that of the standards (analysed at 5 μm × 5 μm), a correction was applied to their isotopic composition (see supplementary material for details). As analyses showed homogenous images of ^{18}O and ^{35}Cl in RTI mode; no electronic gating was used. Pulse height detection (PHD) adjustment was carried out at the start of each day for ^{18}O, ^{35}Cl and, ^{37}Cl and every few days for $^{40}Ca^{19}F$ to account for detector ageing. The external coils were optimised to eliminate mass discrimination at the entrance slit. Terrestrial apatite standards (Ap003, Ap004, Ap018, Ap020; see McCubbin et al., 2012) were used for calibration purposes in this study. Ap004 ($\delta^{37}Cl$ value of ~+0.11‰; Barnes et al., 2016) was used to correct for instrumental mass fractionation of the measured isotope ratios and together with Ap003, Ap018 was analysed to produce a calibration curve of known Cl abundance vs. $^{35}Cl/^{18}O$ ratio from which the eucrite apatite Cl contents were calculated. Although the Cl isotopic composition for Ap003 and Ap018 are unknown and these standards were only used for abundance calibration, their isotopic composition was measured for further monitoring of instrument performance. Supplementary Table 1 provides the average Cl isotopic composition and 2σ standard deviation of these standards relative to Ap004. Supplementary Fig. 2 shows the reproducibility of the $\delta^{37}Cl$ values measured on apatite standard Ap004 across one day (Fig. SM2a) as well as five analytical sessions (Fig. SM2b). Ap020 was used to assess the reproducibility of $\delta^{37}Cl$ values at low Cl contents (see supplementary material). A nominally anhydrous San Carlos olivine and eucrite pyroxene grains located close to the analysed apatite were used to assess the total background Cl contribution. The total background Cl was found to be less than 2 ppm for all sessions (typically 0.2–0.8 ppm). The background contribution to the measured results was <7%, and typically 0–2%, so unless the Cl background had an extreme isotopic composition, it would have a negligible effect on the measured ratios. The Cl isotopic composition of Ap020 (noted for its low Cl content; McCubbin et al., 2012) was analysed to investigate the reproducibility at low Cl concentrations and found to be within error of typical terrestrial values when compared to Ap004

(Fig. SM3, average value $\delta^{37}Cl - 1.21 \pm 8.9‰$, 2σ $n = 8$, uncertainties are high owing to poor counting statistics on low abundance samples). There is, therefore, no evidence for an extreme isotopic composition of the background and as such no correction for background contribution was conducted.

3.3. Electron Probe Microanalysis (EPMA)

Apatite grains were analysed using the Cameca SX100 at The Open University. The beam conditions used were similar to those recommended by Goldoff et al. (2012) (10 kV, 4 nA), to minimise the potential mobilisation of volatile elements and have been previously used at the Open University to measure apatite (e.g., Tartèse et al., 2014). The beam diameter used for analyses was 5 μm.

There has been some discussion in the literature regarding the effects of exposing an apatite grain to a high-current electron beam, such as those typical of routine analysis of major rock-forming minerals by SEM or EPMA and whether this may mobilise the volatiles within and/or out of the apatites crystal structure (e.g. Stormer et al., 1993; McCubbin et al., 2010; Goldoff et al., 2012; Barnes et al., 2013; Stock et al., 2015). Stormer et al. (1993) first demonstrated that both F and Cl X-ray intensities increase during analysis and that this effect was strongly anisotropic, though later work by McCubbin et al. (2010) observed constant Cl rates throughout analyses.

To minimise the mobilisation of F, it was measured first in isolation on a PCO crystal. The crystal was then rotated out of position and the remaining elements were analysed together. Calibration standards used for these analyses include jadite (Na), strontium fluoride (F), bustamite (Mn, Ca), yttrium phosphate (Y, P), tugtupite (Cl), cerium metal (Ce), barite (S), haematite (Fe), forsterite (Mg), feldspar (Si). A secondary apatite standard was analysed prior to analysing unknowns and compared to its known chemical composition to ascertain precision and reproducibility (accuracy better than 2.9% for all elements other than F which was better than 9.7%; reproducibility better than 0.43 wt.% 2σ).

For major elements in the surrounding mesostasis area, a 20 kV accelerating voltage and 20 nA beam current with a 10 μm spot size were used. The elements of interest were calibrated against in-house EPMA standards: for pyroxene, diopside (Ca, Mg, Si), kaersutite (Al), rutile (Ti), rhodonite (Mn) and fayalite (Fe); for plagioclase, anorthite glass (Si, Al, Ca), oligoclase (Na), kaersutite (Mg), orthoclase (K); for chromite, ilmenite and oxides, chromite (Al, Cr, Fe, Mg), diopside (Ca, Si), rutile (Ti), vanadium metal (V), and rhodonite (Mn).

3.4. Zinc isotope analysis protocol

Zinc isotope compositions of bulk DaG 945 were measured using a Thermo Scientific Neptune Plus Multi-Collector Inductively-Coupled-Plasma Mass-Spectrometer (MC-ICP-MS) at the Institut de Physique du Globe in Paris (IPGP) following a well-defined protocol (Chen et al., 2013; Moynier and Le Borgne, 2015; Pringle et al., 2017). Approximately 100 mg of sample powder was dissolved in conc. HNO_3/HF and heated at 130 °C in PTFE containers. Subsequently, the samples were dried down and 5 ml of 6N HCl was added to the residue before heating again to dissolve remaining fluoride complexes. The sample was then dried down again. The chemical purification of Zn was achieved by anion exchange chromatography whereby samples were re-dissolved in 1.5N HBr and then loaded onto AG-1 X8 (200–400 mesh) columns. Matrix elements were removed by further addition of 1.5N HBr and Zn was eluted using 0.5N HNO_3. This process was then repeated on smaller 0.1 mL columns to further purify Zn. The collected solution was then heated to dryness and subsequently taken up in 0.1N HNO_3 for mass spectrometry analysis.

Masses ^{62}Ni, ^{63}Cu, ^{64}Zn, ^{65}Cu, ^{66}Zn, ^{67}Zn and ^{68}Zn were collected on Faraday cups. Isobaric interference from ^{64}Ni was controlled and corrected for by measuring the intensity of the ^{62}Ni peak. Assuming that the ^{64}Ni/^{62}Ni ratio is natural (0.2548) the real ^{64}Zn value can be calculated by;

$$^{64}Zn_{Real} = {}^{64}Zn_{measured} - {}^{64}Ni = {}^{64}Zn_{measured} - \left(\frac{^{64}Ni}{^{62}Ni}\right)_{Natural} \times {}^{62}Ni_{measured}$$

External precision for these measurements is 0.04‰ for δ^{66}Zn (2σ) (Pringle et al., 2017). Results are reported as permil (‰) deviations from the JMC-Lyon (Moynier et al., 2017) Zn isotope standard using the following equation.

$$\delta^{X}Zn = \left[\frac{(^{x}Zn/^{64}Zn)_{Sample}}{(^{x}Zn/^{64}Zn)_{JMC-Lyon}} - 1\right] * 1000$$

where $\times$ = 66, 67, or 68.

4. RESULTS

A total of 33 measurements from 24 individual apatite grains from seven samples were obtained, the data for which are listed in Table 2 and plotted in Fig. 1. EPMA data for apatite grains and the surrounding phases are provided in the supplementary material (Table SM2, SM3). Zinc isotope data for DaG 945 along with literature values for other samples investigated in this study are provided in Table 3.

The chlorine contents of apatite grains studied here display a significant range, from ~24 to ~4900 ppm Cl (given as ppm by weight hereafter). In basaltic eucrites, apatite grains contain similar amounts of Cl with Millbillillie having a relatively restricted range from ~1830 to ~2030 ppm Cl (comparable to our EPMA results, Table SM1) and both DaG 844 and Stannern containing ~1500 ppm Cl. For Stannern these results are comparable to SIMS results of Sarafian et al. (2017b) but ~500 ppm lower than the EPMA results of Sarafian et al. (2013).

The cumulate eucrite Moore County displays a larger range in Cl content, from ~110 to ~690 ppm, which are within the range measured by EMPA during this study (Table SM1), but are almost an order of magnitude lower than results of previous studies (Sarafian et al., 2013). Considerable intra-grain variability in Cl abundance is also

Table 2
δ^{37}Cl values, Cl content, and the associated (2σ) uncertainties for apatite in eucrites. Also reported are areas (raster sizes) for each measurement.

Sample ID	δ^{37}Cl (‰)	2σ (‰)	Cl content (ppm)	2σ (ppm)	Raster size (μm)
Basaltic Eucrites					
DaG 844					
Ap1	2.35	1.18	1444	19	4
Millbillillie					
Ap1	0.26	0.82	2037	26	5
Ap2	3.03	0.88	1921	25	4
Ap3a	−1.49	1.31	2005	26	5
Ap3b	0.08	1.20	2012	26	5
Ap4	−0.53	1.18	1831	24	5
Stannern					
Ap1	3.57	1.42	1490	97	4
Ap2	3.45	1.39	1537	100	5
Cumulate Eucrites					
Moore County					
Ap1	9.31	3.41	113	2	4
Ap2	6.26	1.78	600	10	4
Ap3a	4.75	2.26	692	6	4
Ap3b	6.82	2.47	420	4	3
Ap3c	4.22	2.69	334	3	5
Ap4	13.1	3.01	130	1	3
Residual Eucrites					
Agoult					
Ap1a	8.96	6.66	32	0.5	5
Ap1b	11.6	7.24	25	0.4	5
Ap2	1.08	7.37	26	0.4	5
Ap3	−2.53	7.40	27	0.3	5
Ap4	−3.98	6.08	44	1.3	5
DaG 945					
Ap1a	29.2	3.81	57	1	5
Ap1b	31.5	3.86	47	2	5
Ap2a	27.2	4.40	52	1	5
Ap2b	27.6	3.48	60	3	5
Ap3a	32.2	5.15	32	1	5
Ap3b	35.0	5.08	36	1	5
Ap4	39.2	6.18	24	1	5
NWA 2362					
Ap1a	8.55	0.91	4468	41	4
Ap1b	4.27	0.87	4256	39	5
Ap2	9.32	1.64	2324	43	5
Ap3	8.82	1.54	4142	77	4
Ap4a	16.3	1.54	3921	73	4
Ap4b	11.1	1.52	4897	91	4
Ap5	12.3	1.54	4222	78	4

observed in Moore County with a single grain having a range of ~360 ppm (Ap3). Residual eucrites Agoult and DaG 945 have the lowest Cl contents measured in this study and show restricted variation, both inter-grain as well as intra-grain, with values ranging from ~25 to ~60 ppm (Fig. 1). NWA 2362, however, has the highest Cl content measured for any eucritic apatite in this study as well as a significant inter-grain (~2320 to ~4900 ppm Cl) and intra-grain (~1000 ppm Cl in Ap4) variations; these results consistent with EPMA measurements (Table SM1).

The δ^{37}Cl values obtained for apatite from the basaltic eucrites (DaG 844, Millbillillie, and Stannern) are typically within error of terrestrial values and chondrites or slightly more fractionated in their isotopic composition. Apatite grains within Stannern are very consistent with regards to their isotopic composition, both plotting with δ^{37}Cl values of ~+3.5‰ and are similar to the $+2.35 \pm 1.18$‰ value obtained for DaG 844. Apatite grains within Millbillillie display a somewhat larger range of Cl isotope composition (ranging from -1.49 ± 1.13‰ to $+3.03 \pm 0.88$‰ 2σ) but still broadly consistent with terrestrial and chondritic values, having only one data point outside the error envelope.

The δ^{37}Cl values in Moore County are typically more fractionated than those of basaltic eucrites ($+4.22 \pm 2.69$ to $+13.1 \pm 3.01$‰ 2σ), however, the values also display larger uncertainties, owing to poorer counting statistics related to the lower Cl contents of some apatite grains, and are typically within error of the basaltic eucrites (Fig. 1). Moore

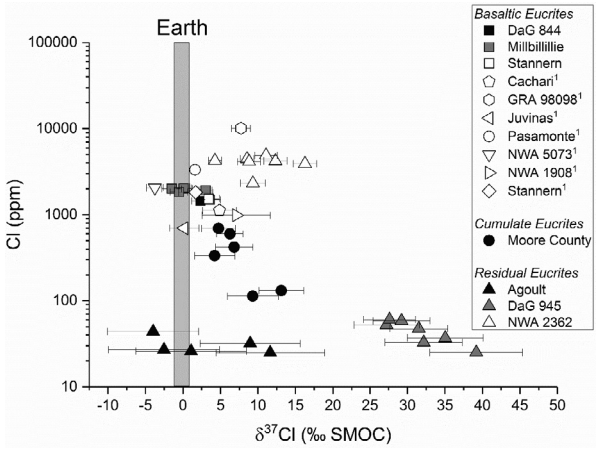

Fig. 1. Plot showing Cl content versus δ^{37}Cl values of apatite in the studied eucrites. [1]Average data from Sarafian et al. (2017b). The vertical grey bar is the terrestrial range (−0.2 ± 1.0‰, Sharp et al., 2013b).

County does, however, have two grains which are significantly more fractionated than the basaltic eucrites and terrestrial values (+9.31 ± 3.41‰ and +13.1 ± 3.01‰ 2σ) and correspond to the lowest Cl content for this sample (113 and 130 ppm Cl, respectively).

The residual eucrites display a wide range of chlorine isotope compositions and are typically higher in δ^{37}Cl than the basaltic eucrites. Agoult has the largest range of δ^{37}Cl values observed in this study, from −3.98 ± 6.08‰ to +11.6 ± 7.24‰ (2σ). The large uncertainties observed in Agoult are, as with Moore County, owing to poorer counting statistics associated with low Cl abundance. Of the five data points from Agoult, three are within error of the majority of basaltic eucrites and the terrestrial range (Fig. 1). Two data points, however, have fractionated δ^{37}Cl values (+8.96 ± 6.66‰ and +11.64 ± 7.24‰ 2σ) similar to Moore County, that lie outside of the terrestrial range but within error (owing to the large uncertainties) of some basaltic eucrites (Fig. 1). All apatite studied in NWA 2362, exhibit a resolvable fractionation in δ^{37}Cl values when compared to the basaltic eucrites and terrestrial values, with values ranging from +4.27 ± 0.87 to +12.3 ± 1.54‰ (2σ) and one value even higher at +16.3 ± 1.54‰ (2σ) (Fig. 1). These values are similar to the heavy Cl values observed in Moore County and Agoult. Whilst Agoult and NWA 2362 have elevated δ^{37}Cl values when compared to the terrestrial range, DaG 945 shows an even more significant fractionation with δ^{37}Cl values ranging from ~+27 ± 4.4‰ to ~+39 ± 6.2‰ (2σ). The δ^{37}Cl values of apatite from DaG 945 are amongst the highest chlorine isotopic compositions recorded for any Solar System material. Repeat analyses of DaG 945 apatite (DaG 945 Ap1 and Ap2) in a separate analytical session confirmed the heavy δ^{37}Cl composition of apatite in this sample. The weighted average δ^{37}Cl value of all apatite grains from this study (+5.3 ± 2.3‰; $n = 33$, 95% confidence) is outside of the terrestrial range (−0.2 ± 1.0; Fig. 1). When combined with the data of Sarafian et al. (2017b) to give a weighted average δ^{37}Cl of +1.70 ± 0.71‰ ($n = 127$, 95% confidence) there is still a small but resolvable difference.

δ^{66}Zn, δ^{67}Zn and δ^{68}Zn compositions of DaG 945 are +13.45‰, +20.15‰ and +26.70‰, respectively. These values are significantly higher compared to other HED meteorites studied by Paniello et al. (2012) (Table 3).

5. DISCUSSION

The dataset generated by this work appears to indicate that more than one process is involved in the petrogenesis of the eucrites studied. In the discussion below, several scenarios are discussed as to how these isotopic values could have been produced.

5.1. Petrology, mesostasis mineral compositions, and bulk elemental abundance

As mentioned in the previous section, the basaltic eucrites have apatite Cl isotopic compositions that range between 0‰ and +3.5‰ with an appreciable amount of Cl (~1500–2000 ppm) whilst cumulate and residual eucrites display a larger range in isotopic composition (+4.22‰ to +13.1‰ for Moore County and −3.98‰ to +39.2‰ for residual eucrites, respectively) at relatively lower Cl contents (<700 ppm, excluding NWA 2362). The variation observed here both inter- and intra-grain are of similar magnitude, or less, than the data published by Sarafian et al. (2017b) conducted on a different instrument and with one sample in common (Stannern). Data for the Moon also show similar levels of variation (e.g. Boyce et al., 2015; Potts et al., 2018).

The petrologic context of apatite grains in basaltic eucrite Millbillillie are similar across the entire sample, being associated with ilmenite and chromite, and except for one data point (Ap2) have similar isotopic compositions and abundance. Whilst Ap2 does not have an obvious difference in petrological context and a similar Cl abundance, there is, however, a resolvable isotopic composition enrichment at +3.03 ± 0.88‰ (2σ).

Table 3
Table displaying the zinc isotopic compositions of samples studied here.

Sample	δ^{66}Zn	δ^{67}Zn	δ^{68}Zn	Zn (ppm)	Ref.
DaG 945	13.45	20.15	26.70	0.5	This Study
Millbillillie	−0.79		−1.37	0.90	Paniello et al. (2012)
Stannern Chip 1	1.42		2.90	1.00	Paniello et al. (2012)
Stannern Chip 2	0.95		2.05	7.80	Paniello et al. (2012)
Mean Stannern	1.19		2.48		Paniello et al. (2012)

The apatite grain analysed in DaG 844, in contrast to Millbillillie and Stannern, occurs interstitial to two large pyroxene grains. Despite its different petrological context the grain has a δ^{37}Cl value of $+2.35 \pm 1.18$‰, +2 to +3‰ higher than most grains and similar to Stannern and Ap2 in Millbillillie. The Cl abundance of this grain (1444 ppm) is also comparable to Stannern (1490–1537 ppm). The H_2O abundance of apatite in DaG 844 and two of three Stannern grains, are significantly higher than those seen in Millbillillie (Barrett et al., 2016). It has been suggested that the relative timing of apatite crystallisation affects the volatile content, with apatite displaying a clear preference of F over Cl and Cl over OH, and therefore, early crystallising apatite would have higher F/OH ratio than later formed apatite (Boyce et al., 2014; McCubbin et al., 2015). If the pre-requisites of McCubbin and Jones (2015) were met, Millbillillie with its higher Cl content and lower, more variable H_2O content of apatite, may represent an earlier phase of crystallisation relative to DaG 844 and Stannern.

One grain in Stannern (Ap2) has a noticeably different texture when compared to other apatite studied in this meteorite and the rest of basaltic eucrites. This grain appears to have co-crystallised with the silicates surrounding it even including small amounts of other minerals within the crystal (Fig. SM1 Stannern SOI2). Despite this different texture, the grain has a similar Cl abundance and isotopic signature to that of the other grain analysed in Stannern (Ap1). Barrett et al. (2016) noted that this particular grain contained less H_2O than other Stannern apatite analysed and could represent an earlier-formed apatite within Stannern, consistent with the evolution of apatite chemistry during fractional crystallisation where earlier crystallised apatite is F-rich and OH-poor and late-crystallising apatite is more OH-rich (Boyce et al., 2014; McCubbin et al., 2015). Moore County apatite grains, on the other hand, do not appear to show significant petrological differences between the grain with heavier (13.1‰) and lighter (4.22‰) δ^{37}Cl values. Apatite grains here are similar in texture to those described by Sarafian et al. (2013) though the abundance of volatiles, both Cl and H_2O, are significantly lower than previously reported in the literature. It is possible that Moore County reflects a very localised process rather than larger scale processes such as the mixing of different reservoirs as has been suggested on the Moon (e.g. Barnes et al., 2019).

The residual eucrites Agoult and DaG 945 share some petrological similarities but appear to be somewhat distinct from NWA 2362. Apatite in all of the samples are typically associated with relict mesostasis regions, but Agoult and DaG 945 apatite appear to have a stronger association with minerals such as chromite, ilmenite and a silica phase and the overall meteorites are more granulitic than NWA 2362. Agoult apatite are located in separate regions with no obvious spatial relationship between the light and the heavy Cl results. DaG 945, on the other hand, displays a consistently heavy Cl isotopic composition throughout the thin section. In NWA 2362, Ap2 stands out as anomalous with regards to its Cl content, almost 2000 ppm lower in abundance than the rest of the grains analysed. This grain, however, would appear to have a similar petrological context as the rest of the analysed grains, though it is closer to cracks filled with likely terrestrial FeO (Fig. SM1). Any removal of Cl from this apatite grain by terrestrial weathering would likely have altered the Cl isotopic composition. As this grain has a consistent δ^{37}Cl with respect to other grains within this sample it would seem unlikely that terrestrial alteration lowered the Cl abundance without compromising its isotopic composition. Two other apatite grains in NWA 2362 (Ap 1 and Ap4) show significant heterogeneity with regards to their Cl isotopic composition. The data points in Ap4 are also variable in Cl abundance with the higher Cl isotopic composition associated with the lower abundance ($+16.3 \pm 1.55$‰ and 3921 ppm, vs. $+11.1 \pm 1.52$ and 4897 ppm Cl). There is no obvious difference in the petrological context of these grains when compared to other NWA 2362 grains and the general intra-grain consistency of other apatite analysed within this study would suggest that this heterogeneity is real. As the residual eucrites have all experienced high degrees of thermal metamorphism and the extraction of partial melts (Yamaguchi et al., 2009), it is possible that the degree of melt extraction could have affected the Cl content and isotopic composition, which is discussed later in Section 5.4.

In the case of lunar apatite in mesostasis regions, Potts et al. (2016) note that the development of individual melt pockets exerts a greater control on the composition and texture of the mesostasis region than the bulk. Any changes in the chemistry of minerals surrounding apatite could, therefore, highlight differences in crystallisation conditions between apatite grains and potentially explain the variation observed. As such, the chemical compositions of mineral phases surrounding the apatite grains were analysed but no obvious systematic variations could be correlated to δ^{37}Cl values for any sample (Table SM3). The surrounding mineral phases all have typical compositions in terms of major elements for eucrites of their type and are broadly consistent with published literature values (e.g. Yamaguchi et al., 2009; and supplementary material of Mittlefehldt, 2015). Interestingly, the basaltic eucrites all contain merrillite (though only in the DaG 844 section studied here was merrillite and apatite observed in close proximity to one another) but merrillite was not observed in the other samples in this study. All of the basaltic eucrites have consistently low and invariant δ^{37}Cl values and very similar Cl contents compared to the more variable Cl isotope signatures in residual and cumulate eucrites (Table 2). Similarly, Sarafian et al. (2017b) did not observe correlations between the presence and/or absence of merrillite and δ^{37}Cl values in basaltic eucrites: NWA 1908 and NWA 5073 both have distinctly non-zero δ^{37}Cl values (average values of $+7.10 \pm 4.57$‰ and -3.75 ± 1.14‰, respectively) and a much larger range in Cl content (988 ppm and 2058 ppm Cl respectively; Sarafian et al., 2017b). It should be noted, however, that NWA 5073 contains olivine veins which indicate this sample could potentially be a highly metasomatised eucrite (Barrat et al., 2011; Roszjar et al., 2011; Warren et al., 2014). As no sample studied here displays evidence of metasomatism (e.g. veining), this can be effectively ruled out as a mechanism

for fractionation of Cl (and Zn) isotopes. The metamorphic grade, indicated using the pyroxene classification of Takeda and Graham (1991) and expanded upon by Yamaguchi et al. (1996), also shows no correlation with either the Cl abundance or the Cl isotopic signature of the meteorite.

In a recent study, Sarafian et al. (2017b) observed a correlation between major and trace elements plus halogen content with δ^{37}Cl and suggested that this was related to degassing of the vestan magma ocean or, alternatively, during emplacement or eruption after the magma ocean phase. Fig. 2 displays the bulk rock abundances for various elements plotted against apatite δ^{37}Cl values. The figure shows that there are very weak or no correlations between bulk major elements, and δ^{37}Cl and correlation improves somewhat if DaG 945 is excluded (DaG 945 is excluded based on its large leverage (HI) values in a simple linear regression model. See supplementary material and Tables SM4, SM5 for more details). Sarafian et al. (2017b) suggested a negative relationship between both Mg and Cr and δ^{37}Cl owing to the crystallisation of olivine and spinel during magma ocean crystallisation, respectively. Similarly, their positive relationship between Sc and δ^{37}Cl implied that olivine rather than pyroxene was a major phase during magma ocean crystallisation. The weak correlation observed between bulk K and apatite δ^{37}Cl could represent the coupled loss of K and Cl during degassing as KCl (Sarafian et al., 2017b). DaG 945, however, is an obvious outlier in Fig. 2 with an appreciable amount of K and significant enrichment in Cl isotopic signature. This anomalous signature could potentially be caused by the degassing of KCl being suppressed by an element that is more reactive with Cl in the melt from which this sample formed. As these samples are a mixture of meteorite finds and observed falls, it is unlikely that terrestrial weathering could be the cause of the observed correlation.

5.2. Degassing of metal chlorides

In the case of the Moon, there are currently two main models proposed for the fractionation of Cl isotopes; (i) the degassing of Cl, in the absence of H, as metal chlorides from lunar mare magmas (Sharp et al., 2010b; Ustunisik et al., 2015) and (ii) degassing of metal chlorides from the lunar magma ocean (Boyce et al., 2015) or urKREEP (Barnes et al., 2016). If degassing had played a significant role then there are several characteristic features that should be observed in apatite as outlined below (Sharp et al., 2010b; Boyce et al., 2015; Barnes et al., 2016): (1) Elevated ^{37}Cl/^{35}Cl ratios should be inversely proportional to Cl abundance. (2) Elevated ^{37}Cl/^{35}Cl ratios should not be observed in samples with abundant H (Schauble et al., 2003; Sharp et al., 2010a, 2010b). (3) Elevated ^{37}Cl/^{35}Cl

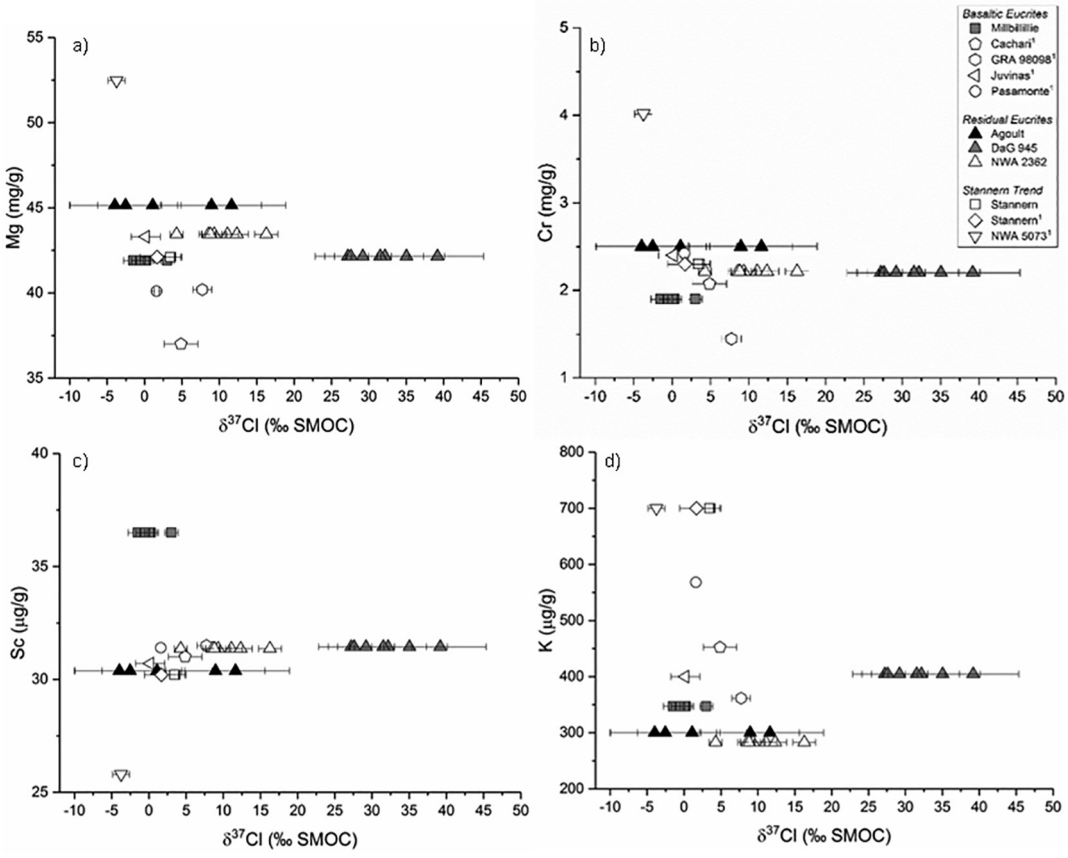

Fig. 2. Bulk elemental data versus average δ^{37}Cl values for (a) Mg, (b) Cr, (c) Sc, (d) K. Note there is no significant correlation between either Mg, Cr, Sc, and average δ^{37}Cl. K does appear to have a weak negative correlation if DaG 945 is excluded as an outlier. Average δ^{37}Cl values from Sarafian et al. (2017b) indicated with a[1]. See supplementary material for references pertaining to the bulk rock compositions.

ratios should be observed only in samples that have high D/H ratios. Mesostasis pockets in partially solidified lunar magmas can evolve differently (Pernet-Fisher et al., 2014) meaning apatite saturation would occur at different times and the solubility of Cl (and H) may be different in various mesostasis pockets. With regards to eucrites, Sarafian et al. (2017b) suggest that observed Cl isotope fractionation occurred during degassing of the vestan magma ocean and also assumed that Cl and H species degassed at the same time. These authors demonstrate that mixed degassing of $H_2 + H_2O$ can reduce H content without significant isotopic fractionation owing to these species fractionating H isotopes in opposite directions (H_2 degassing leads to D-rich melt with a fractionation factor (α) = 0.816, H_2O degassing leads to D-poor melt $\alpha = 1.049$; Newman et al., 1988; Sharp et al., 2013a). This phenomenon has been used to also explain the observations from angrites, where ~80% H_2O was lost with little H isotope fractionation (Sarafian et al., 2017a). It has been recently demonstrated experimentally that during volatile-rich magma ascent, H is one of the earliest volatiles to degas and a H-rich vapour would be lost at a faster rate than a Cl-rich vapour (Ustunisik et al., 2015). Once depleted in H, Cl would subsequently become the preferred volatile to degas and would suggest that H and Cl isotope systematics are decoupled (Sharp et al., 2013a; Ustunisik et al., 2015).

The relationship between Cl and H for the eucrites analysed in this study is shown in Fig. 3. As presented in Fig. 1, samples with low Cl content typically have higher $^{37}Cl/^{35}Cl$ ratios. Fig. 3 also demonstrates the lack of relationship between $\delta^{37}Cl$ values, Cl content, and H_2O abundance suggesting the Cl and H systems could be decoupled from each other. Unfortunately, there are no hydrogen isotope or H_2O content data available for Agoult or NWA 2362. In all samples, apatite grains display almost invariant δD values (Sarafian et al., 2014; Barrett et al., 2016) but a range of $\delta^{37}Cl$ values. As shown in Fig. 3, low $\delta^{37}Cl$ values are observed over the entire range of H_2O contents, but high $\delta^{37}Cl$ values appear only below 500 ppm H_2O. One apatite crystal in DaG 945 (Ap3) displays a 4-fold variation in H_2O abundance (60 and 229 ppm H_2O; Barrett et al., 2016), however, the Cl isotope analyses were only co-located with one of the H isotope analysis areas (Fig. SM1). The variation in H_2O abundance across a grain is probably caused by heterogeneity in the apatite crystal and so the value from the closest H isotope pit is used (229 ppm) in Fig. 3 (it should be noted that using either measurement would not change the conclusion presented here). DaG 844 and one of the two apatite grains in Stannern are characterised by high H_2O content (>1100 ppm H_2O) and $\delta^{37}Cl$ values of ~+3‰. As mentioned in the previous section, however, one grain in Stannern (Ap2) studied here has a low H_2O content (~35–45 ppm H_2O; Barrett et al., 2016) and is also characterised by a slightly enriched $\delta^{37}Cl$ value of +3.45 ± 1.39‰. The apatite in Moore County and DaG 945 also display low H_2O contents (typically <200 ppm), with DaG 945 showing more variability than Moore County in terms of H_2O content. Both of these samples display some of the heaviest $\delta^{37}Cl$ values. Results from this study broadly agree with the first two of the characteristic features outlined at the start of this section but disagree with the third and final characteristic. It is possible that the mixed $H_2 + H_2O$ degassing scenario (Sarafian et al., 2017b) resulted in the low H_2O content with invariant D/H ratios. This sequence of H (presumably a mixture of $H_2 + H_2O$ to avoid D/H fractionation; Sarafian et al., 2017b) followed by subsequent Cl degassing would appear to fit the eucrites, as the basaltic eucrites studied here contain relatively low H_2O contents with unfractionated D/H ratios. The subsequent degassing of Cl as metal chlorides in a low H environment could then account for the variation observed in Cl isotopes.

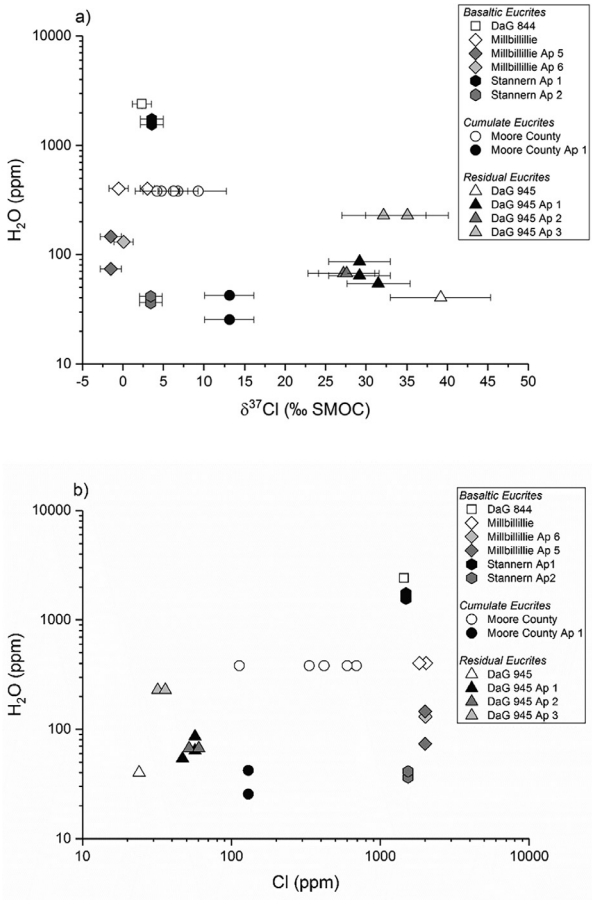

Fig. 3. (a) Plot of $\delta^{37}Cl$ values versus H_2O content. (b) Plot of Cl content versus H_2O content. Solid symbols indicate apatite grains where both *in-situ* chlorine and hydrogen isotope measurements have been obtained from the same apatite grain. Open symbols indicate apatite grains where no hydrogen isotope measurements have been obtained and, therefore, average H_2O values for the entire sample were used. H_2O abundances are from Barrett et al. (2016).

There appears to be a positive correlation between apatite $\delta^{37}Cl$ and bulk $\delta^{66}Zn$ (Fig. 4). While Zn isotopes do not fractionate significantly during magmatic emplacement and differentiation (only 0.07‰, Chen et al., 2013; Sossi et al., 2018) they are highly fractionated during evaporation processes (e.g., Moynier et al., 2009; Day et al., 2017a, 2017b). The enriched $\delta^{66}Zn$ and $\delta^{37}Cl$ combined with low Cl and H_2O abundance of DaG 945 compared to basaltic eucrites,

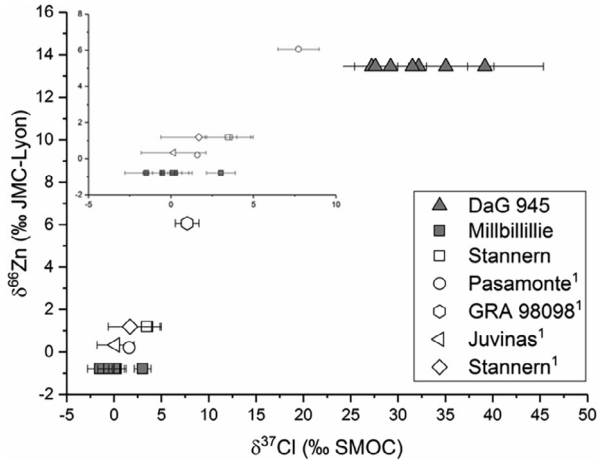

Fig. 4. Plot of bulk $\delta^{66}Zn$ values versus $\delta^{37}Cl$ values from apatite. [1]Average apatite values from Sarafian et al. (2017b). Insert displays the same plot without DaG 945. The Zn isotope data are taken from Paniello et al. (2012).

which contain significantly more H_2O and Cl and display relatively unfractionated $\delta^{66}Zn$ and $\delta^{37}Cl$ values, appears to support the hypothesis that Cl could have degassed as metal chlorides (Paniello et al., 2012; Sarafian et al., 2017b). Graves Nunataks (GRA) 98098, however, does not follow this trend containing the highest Cl abundance of eucrites to date but is also enriched in heavy isotopes for both Cl and Zn. As such a different process is required to explain the $\delta^{37}Cl$ values of GRA 98098.

To test the degassing hypothesis further, simple degassing modelling was undertaken using the Rayleigh fractionation relationship $R = R_0 \times f^{(\alpha-1)}$, where R_o and R are the initial and final $^{37}Cl/^{35}Cl$ ratios of chlorine in the melt, respectively, α is the fractionation factor and f is the fraction of chlorine remaining in the melt. Fig. 5 shows degassing curves for a variety of metal chloride species assuming an initial $\delta^{37}Cl$ of 0‰. Based on this model basaltic eucrites studied here appear to be relatively undegassed. The slightly

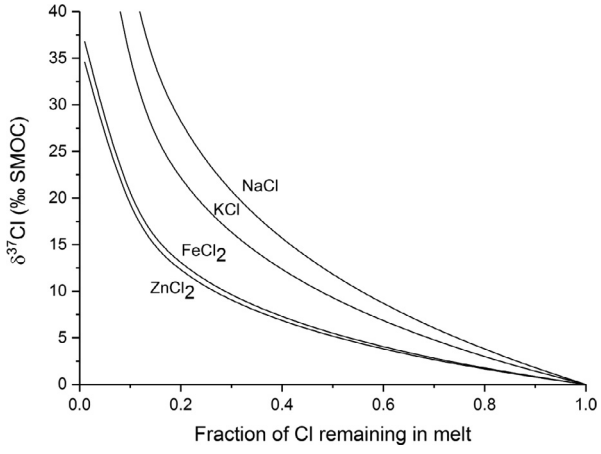

Fig. 5. Calculated degassing trajectories of various metal chloride species: assuming an initial $\delta^{37}Cl$ value of 0‰. The calculation of these curves are outlined in the text.

^{37}Cl-enriched values observed by Sarafian et al. (2017b) in Stannern ($\delta^{37}Cl + 1.69 \pm 2.30$‰), Cachari ($\delta^{37}Cl$ 4.87 $\pm$ 2.25‰), and anomalous eucrite Pasamonte ($\delta^{37}Cl$ + 1.60 $\pm$ 0.32‰), require between roughly 10–50% degassing depending on the metal chloride species. If apatite in a single sample shared a common degassing event, the inter-grain variation observed could potentially be explained by grains crystallising at different times during the same event.

Apatite in the residual eucrite DaG 945 have $\delta^{37}Cl$ values of ~+30‰ and low H_2O abundances (~50 to ~150 ppm H_2O; Barrett et al., 2016) which could indicate loss of Cl in a H-poor environment at the time of degassing (Sharp et al., 2010b; Boyce et al., 2015; Barnes et al., 2016). Given that DaG 945 $\delta^{66}Zn$ values are also significantly fractionated (Fig. 4; it should be noted that the calculated leverage (HI) values for this sample do not suggest it is an outlier and the p-value is <0.05), this could suggest $ZnCl_2$ was one of the degassing phases for this sample and that >95% degassing had occurred. It is difficult to ascertain whether Agoult has undergone any degassing owing to the large uncertainties associated with its $\delta^{37}Cl$ values. Whilst the lightest Cl isotope value from this sample (−3.98 $\pm$ 6.08‰) does have the highest Cl content, at 44 ppm, and the heaviest value has the lowest Cl content (+11.64 $\pm$ 7.24‰ and 25 ppm Cl), the large uncertainties associated with all of the isotopic measurements from this sample precludes any meaningful correlation. Cl isotope values of ~+8‰, similar to that of NWA 2362 can be modelled by moderate amounts of degassing with a range from 38% to 66% Cl vapour loss, depending on the degassing species. Ap4 in NWA 2362 records heterogeneous Cl isotope values and contents. Since the more fractionated $\delta^{37}Cl$ value is associated with the lower of the two measured Cl contents, it could potentially be an example of an apatite that crystallised during degassing. Ap1 from the same sample, however, does not show the same correlation. Without knowing the orientation of the crystal it is not possible to know if this intra-sample variation represents a loss of Cl from core to rim.

In contrast to the basaltic and residual eucrites, Moore County displays a more variable Cl isotope composition with a correlation between decreasing Cl content and increasing $\delta^{37}Cl$ values (Fig. 1). As this sample is a cumulate eucrite and is likely to have formed at depth, conventional wisdom would suggest that it is unlikely to have suffered any significant magmatic degassing. Recent work by Wales and Boyce (2016) documents the loss of H from apatite in terrestrial intrusions which could lead to isotopic fractionation. These authors suggest that caution should be taken when interpreting intrusive rocks in terms of degassing. Owing to the aforementioned variability of the Cl isotope composition and negative correlation between Cl content and $\delta^{37}Cl$ it is possible that Moore County may have degassed Cl. Similar to DaG 945, the apatite grains analysed in this study for Moore County also have a low H_2O abundance (25 to ~125 ppm H_2O; Barrett et al., 2016) and may have degassed chlorine in a hydrogen-poor environment. These low H_2O abundances for Moore County, however, are in stark contrast to the ~0.6 wt.%

H_2O measured by SIMS in Sarafian et al. (2013) for apatite with similar petrological context. It would be expected that these apatite grains with high H_2O content would have unfractionated Cl isotopic compositions (i.e. 0‰).

Eucrite degassing may have occurred relatively early during the formation of Vesta. Paniello et al. (2012) suggested that unbrecciated eucrites represented an early eucritic crust shortly after differentiation and their heavy zinc isotopic signature was owing to the volatilisation of isotopically lighter zinc. For the Moon, Dhaliwal et al. (2017) modelled the loss of Zn during a lunar magma ocean (LMO) phase under various conditions. Their first model yielded a relatively homogenous bulk solid LMO δ^{66}Zn value, while the second resulted in stratification of δ^{66}Zn values within the LMO sequence. This second model could be applied to account for the variation in zinc and chlorine isotopes observed in the eucrite parent body. However, as noted by Boyce et al. (2015), this would suggest later samples would be enriched in incompatible trace elements, something discussed in more detail below in Section 5.3. Degassing during magmatic emplacement/eruption is an alternative hypothesis which can account for the variation seen in eucrites where each sample represents a different flow, some of which degassed (e.g. DaG 945) and some of which did not (e.g. Millbillillie).

Overall the meteorites studied here are consistent with loss of moderately volatile Zn and Cl based on the positive correlation between apatite δ^{37}Cl and bulk δ^{66}Zn shown in Fig. 4, in agreement with the findings of Sarafian et al. (2017b). Given the strong correlation between Zn and Cl isotopes and low H abundance in measured apatite with heavy Cl isotope signatures, it is possible that the $ZnCl_2$ was a degassing phase for Cl, in a H-poor environment. A potential minor component could be KCl owing to a weak negative correlation observed between K and δ^{37}Cl (Fig. 2 and Sarafian et al., 2017b).

5.3. Contamination by 'vKREEP'

An alternative hypothesis is that the Cl isotopic composition is controlled, at least in part, by the addition of an enriched Cl rich component. In the case of the Moon, it is proposed that the later formed cumulates (including the last dregs of the lunar magma ocean (LMO) enriched in incompatible elements such as K, rare earth elements (REEs), and P, collectively called KREEP and its primitive form – urKREEP) acquired heavier Cl, Zn, Ga, and Rb isotopic signatures on account of incompatibility within silicates compared to early formed cumulates with low incompatible trace element abundances and unfractionated Zn and Cl isotopic compositions (Day and Moynier, 2014; Boyce et al., 2015; Kato et al., 2015; Barnes et al., 2016; Kato and Moynier, 2017; Pringle and Moynier, 2017). This enriched reservoir, was later mixed (during cumulate overturn) with earlier formed cumulates with unfractionated Cl, to create the range of values observed among samples of different lunar lithological types (Boyce et al., 2015; Barnes et al., 2016). This contamination by an urKREEP component can be fingerprinted using, for example, bulk La/Sm or La/Yb ratios, where higher La/Sm and La/Yb ratios correspond to increasing contamination (Boyce et al., 2015; Barnes et al., 2016).

Small fragments of a KREEP-like component discovered in two howardite meteorites suggest the possible existence of a 'vestan KREEP' or vKREEP (Barrat et al., 2012). Fig. 6 displays the bulk La/Yb ratio versus δ^{37}Cl of apatite from eucrites. If eucrites were contaminated by a vKREEP component then we would expect to see similar enrichments in heavy Cl and REEs as the lunar samples. As Stannern and the Stannern trend eucrites are characterised by elevated incompatible trace elements, we would also expect these samples to follow the lunar trend and contain enriched Cl isotopic signatures. Stannern shows a slightly enriched bulk La/Yb ratio, compared to the other basaltic eucrites studied here (Fig. 6). GRA 98098 (a main group eucrite from Sarafian et al., 2017b) has a La/Yb ratio between Stannern and the main-group basaltic eucrite Millbillillie, but a heavier Cl signature than Stannern, in keeping with the δ^{37}Cl range of Schneck et al. (2016). Interestingly, NWA 5073 (a Stannern trend eucrite), which has the highest La/Yb ratio, has one of the lowest average δ^{37}Cl observed, possibly owing to metasomatic fluid interactions (Roszjar et al., 2011).

Most basaltic eucrites do not show a significant positive correlation between La/Yb ratio and Cl isotope signature (Fig. 6) to warrant assimilation of a ^{37}Cl-enriched vKREEP component in their petrogenesis (Mittlefehldt and Lindstrom, 2003; Yamaguchi et al., 2009). There does, however, appear to be a negative relationship between La/Yb and δ^{37}Cl values. The low REE values of Moore County can be accounted for using a mixture of crystals and inter-cumulus magma as outlined by Treiman (1997) and Barrat et al. (2000). The residual eucrites, however, all display low La/Yb ratios and have significant variation in Cl isotopic composition with DaG 945 having the lowest observed La/Yb ratio and most elevated δ^{37}Cl values. The

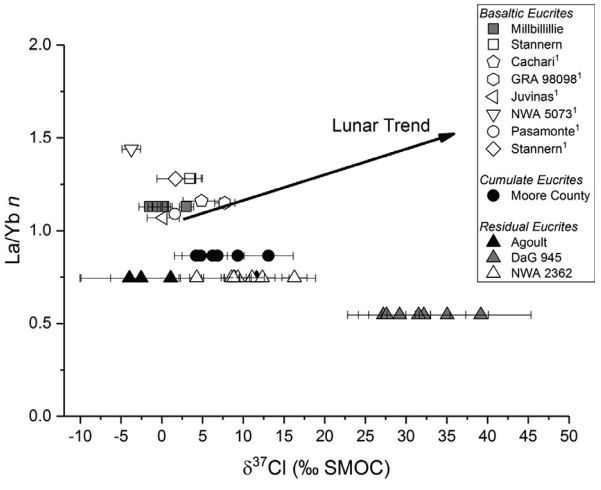

Fig. 6. Plot of bulk La/Yb ratios (normalised to CI chondrites) versus average δ^{37}Cl values of apatite. [1]Average values from Sarafian et al. (2017b). The reference chondrite is from Lodders (2003). The lunar trendline is based on the data of Boyce et al. (2015) and Barnes et al. (2016).

lack of positive correlation suggests that contamination by a ^{37}Cl-enriched vKREEP component is unlikely to cause the variation in δ^{37}Cl values observed here.

5.4. Partial melting and diffusion-controlled isotope fractionation

Yamaguchi et al. (2009) suggested that, residual eucrites lost a partial melt as a result of extreme metamorphism which is indicated by their light REE depletion. The authors proposed that these partial melts could be the contaminant Barrat et al. (2007) required to form the Stannern trend eucrites. As partial melting is known to concentrate Cl at the Earth's surface (Bonifacie et al., 2008) it is also possible this process might cause isotopic fractionation on extraterrestial bodies. If so, then partial melting of these eucrites could have preferentially scavenged isotopically light ^{35}Cl to the melt fraction. Correlations between δ^{37}Cl and La/Yb ratio in cumulate and residual eucrites (Fig. 6), could be accounted for by differing degrees of partial melting or contamination, with DaG 945 having undergone the largest degree of partial melting and NWA 5073 having experienced the most contamination. The high δ^{37}Cl values observed in apatite from Stannern ($\sim$+3.45‰), however, do not appear to fit this hypothesis.

There are problems, however, with this mechanism: at high temperatures Cl is not expected to fractionate significantly (Schauble et al., 2003), and there is no experimental evidence for fractionating Cl isotopes during partial melting, unlike the case with Fe isotopes, where isotopically heavy iron preferentially enters the melt (Weyer and Ionov, 2007), contrary to what would be required to explain the Cl isotope data.

Instead of partial melting directly fractionating Cl, if the crust were partially melted and the melt already saturated with respect to apatite, then the apatite could have exchanged volatiles by diffusion with the melt. Diffusion has the potential to alter the Cl content of the apatite and fractionate Cl isotopes, with ^{35}Cl diffusing faster than ^{37}Cl (Eggenkamp et al., 1994). Experiments conducted at low temperatures in aqueous environments demonstrate that only minor fractionation, up to 2‰ could be produced by diffusion (Eggenkamp and Coleman, 2009), which unsurprisingly decreases with increasing temperature (Eggenkamp, 2014). Recent work, however, by Fortin et al. (2017) on Cl diffusion in dacite melts, suggests fractionations up to $\sim$5‰ are possible during convective bubble growth. This suggests that, even under the most favourable conditions, diffusion-controlled Cl fractionation would lead to at most <5‰ variation of δ^{37}Cl values and could not account for the large variations (>5‰) observed in some eucrites. As no single process adequately explains the observations, it would suggest that more than one process was involved in establishing the final Cl isotopic composition of eucrites.

5.5. Implications for volatiles in the inner Solar System

Sarafian et al. (2017b) presented data for Pasamonte, a sample with a small, yet resolvable, difference in O isotopic composition from basaltic eucrites along with low-level Fe-metasomatism (Barrat et al., 2011) despite being otherwise petrologically and compositionally indistinguishable from them (Wiechert et al., 2004; Greenwood et al., 2005; Scott et al., 2009). This allows for comparison between anomalous eucrites and typical basaltic eucrites. The fact that Pasamonte has a similar volatile content and isotopic signature, for both hydrogen (Sarafian et al., 2014) and chlorine (Sarafian et al., 2017b), suggests that at least these two bodies may have a common source region for their volatiles and have undergone similar processes, or, if Pasamonte also represents a portion of Vesta, that the impactor which caused the variation in O isotopes imparted little in terms of volatiles or had a similar isotopic composition of volatile elements to basaltic eucrites. This would likely make the impactor a carbonaceous chondrite-like (Robert, 2006; Alexander et al., 2012; Sharp et al., 2013b, 2016; Williams et al., 2016).

On a first order estimate, if we assume bulk Vesta accreted from $\sim$75% H-chondrite and $\sim$25% CM-like chondrite (Boesenberg and Delaney, 1997; Toplis et al., 2013) and use their average bulk δ^{37}Cl values (Bridges et al., 2004; Sharp et al., 2007; Sharp et al., 2013b), the initial bulk Cl isotopic composition of Vesta would be $\sim -0.26 \pm 2.05$‰. The lower bound of this estimate could account for some but not all of the negative δ^{37}Cl values observed in eucrites. The combined δ^{37}Cl weighted average of apatite in eucrites ($+1.70 \pm 0.71$‰; $n = 127$, 95% confidence) is, however, within error of this estimated bulk Vesta value. It should be noted, however, that as degassing raises the Cl isotopic composition, samples with lower values are more likely to be representative of the body than those with high δ^{37}Cl values (e.g. DaG 945).

Whilst several works have suggested an inner Solar System δ^{37}Cl of $\sim$0‰ (Magenheim et al., 1994; Sharp et al., 2007, 2013b), other, more recent, studies have considered the possibility that there might be a reservoir of isotopically lighter chlorine with $\delta^{37}\text{Cl} \sim -4$‰ (Bridges et al., 2004; Sharp et al., 2013b, 2016; Williams et al., 2016; Sarafian et al., 2017b; Shearer et al., 2018). This lighter reservoir was interpreted by Sharp et al. (2016) as representative of the primitive solar nebula, and as Mars is known to have accreted faster than the other terrestrial planets (Dauphas and Pourmand, 2011; Bouvier et al., 2018), it could have recorded the primary nebular value within its interior. Bellucci et al. (2017), however, show that the negative δ^{37}Cl values (-5.6‰ to -2.7‰) observed in some martian meteorites are associated with core-rim relationships and increased concentrations in all halogens. These authors interpreted this as a rim resulting from reaction with martian brines and, therefore, no isotopically light nebula need be invoked. These authors also note that phosphates do not show grain-scale heterogeneities and record an isotope composition similar to Earth and chondrites, further calling into question the isotopically light nebula reservoir. This would not, however, account for the light isotopic signature recorded by the LL chondrite Parnallee (-1.36 to -4.25‰; Sharp et al., 2013b) or Chassigny (-4 to -6‰) which preserves the noble gas signature of the martial mantle and is unaffected by fluids (Shearer et al., 2018). As no core-rim

zonation is observed in apatite from eucrites and non-zero $\delta^{37}Cl$ values are not typically associated with increased Cl, reaction of apatite with vestan brines, the light isotopically nebula reservoir is still a possibility. As noted earlier, NWA 5073 which contains olivine veins indicating this sample could potentially be a highly metasomatised eucrite (Barrat et al., 2011; Roszjar et al., 2011; Warren et al., 2014). It is, therefore, possible that the light $\delta^{37}Cl$ values of this sample arise from local fluid effects rather than the mark of a nebula component.

Given the rapid accretion of Vesta (Touboul et al., 2015) and the ^{37}Cl-depleted isotopic signature observed in this study (although the uncertainties associated with these negative values here are large) and the work of Sarafian et al. (2017b) it is also possible that Vesta has recorded this primary nebular value. The chlorine isotopic variation displayed by the majority of eucrites could then be accounted for by different degrees of degassing of a magma ocean and or during basalt emplacement/eruption. Smaller bodies, such as Vesta, would degas more efficiently than larger bodies owing to a greater surface area to volume ratio and coupled with the more rapid accretion time, and lack of atmosphere, could preserve significantly more heterogeneity than larger, more slowly-forming planetary bodies. The escape velocity on Vesta is low compared to larger bodies (0.36 km s^{-1}; Lodders et al., 1998); so the escape of volatiles such as Cl and Zn would be trivial (Day and Moynier, 2014). The Moon is thought to have formed significantly later than Vesta (e.g. Bottke et al., 2015), but still sufficiently early to have incorporated this primitive reservoir during accretion (as shown by the $\delta^{37}Cl - 4‰$ in lunar meteorite MIL 05035; Boyce et al., 2015). Most of the lunar samples display terrestrial-like or ^{37}Cl-enriched compositions (e.g. Sharp et al., 2010b; Boyce et al., 2015; Barnes et al., 2016) though it is possible that material with a lighter isotopic signature, below the MIL 05035 data point, has yet to be discovered.

The strikingly similar volatile content and isotopic composition of the anomalous eucrite Pasamonte (Sarafian et al., 2017b) with basaltic eucrites and terrestrial values, supports a common volatile reservoir and processes for the asteroid belt. This could be further strengthened by the analysis of other anomalous achondrites for their volatile content and isotopic compositions.

6. SUMMARY AND CONCLUSIONS

In general, most Solar System materials exhibit a relatively narrow range in bulk and apatite Cl isotope compositions, with terrestrial rocks, martian and chondritic meteorites having $\delta^{37}Cl$ values of ~ -5.6 to $\sim +1.8‰$. Lunar rocks along with residual eucrite DaG 945, however, appear to be an exception, displaying a significant range in their bulk and apatite $\delta^{37}Cl$ values from -4 to $+40‰$. As eucrites formed very early and are among the most abundant achondrites they can help us to constrain the processes that operated on asteroid parent bodies early in the Solar System history.

In this study the abundance and isotopic composition of Cl in apatite were determined for seven eucrites representing a broad range of textural and petrological characteristics as well as the bulk Zn isotopic composition for one sample. Apatite Cl abundances range over several orders of magnitude from ~25 to 4900 ppm and $\delta^{37}Cl$ values range from -3.98 to $+39.2‰$. Whilst samples with lower measured apatite H_2O content typically were also enriched in $\delta^{37}Cl$ there was no correlation between $\delta^{37}Cl$ and δD values. A strong positive correlation between bulk $\delta^{66}Zn$ and apatite $\delta^{37}Cl$ supports the hypothesis that Cl degassed as metal chlorides, in a hydrogen poor environment.

Based on the results presented here, the following conclusions can be drawn:

- The abundance and isotopic composition of Cl recorded by apatite from basaltic eucrites display a similar range in $\delta^{37}Cl$ values to those reported previously for eucrites (Schneck et al., 2016; Sarafian et al., 2017b). Residual eucrites, particularly DaG 945, display a large range in compositions similar to lunar apatite (e.g. Boyce et al., 2015; Barnes et al., 2016).
- The results obtained here show a weak negative correlation between Cl abundance and $\delta^{37}Cl$ values. Samples enriched in heavy Cl are also relatively H_2O poor. DaG 945 and Moore County display both of these trends and are in keeping with the degassing of metal chlorides in an H-poor environment (Sharp et al., 2010b).
- There is no obvious correlation observed between $\delta^{37}Cl$ and δD values of apatite.
- A strong positive correlation ($R^2 = 0.95$) between bulk $\delta^{66}Zn$ and $\delta^{37}Cl$ is observed suggesting that $ZnCl_2$ could have been a degassing metal chloride. A weaker, negative correlation is observed between bulk K content and $\delta^{37}Cl$ which could suggest contemporaneous KCl degassing.
- When compared with $\delta^{37}Cl$ of apatite, the bulk La/Yb ratios of eucrites appear to follow a trend opposite to that observed for the Moon (Boyce et al., 2015; Barnes et al., 2016), suggesting that contamination of eucritic magmas by a 'vKREEP' component (if that took place) is unrelated to the Cl isotope fractionations recorded in apatite.

Here we present evidence from volatile elements that improves our understanding of the magmatic processes that operated on the HED-parent body ~8 to 20 Ma after CAIs. The data in this study would suggest that multiple processes could be involved in the acquisition of the Cl isotopic composition of eucrites. One possible mechanism of ^{37}Cl isotope enrichment on Vesta could have been the degassing of Cl in the form of metal chlorides. The timing of this degassing, however, remains enigmatic.

ACKNOWLEDGEMENTS

This work was funded by a STFC Studentship to TJB and research grant to MA (ST/I001298/1) and a research grant to BLAC, IAF, MA, MMG, RCG and RT (ST/L000776/1). The following individuals are thanked for providing samples: Alex Bevan (Western Australia Museum, Millbillillie (13357.3)), Ludovic Ferrière (Naturhistorisches Museum Wien, Stannern (L4979)), Linda Welzenbach (Smithsonian Institute, Moore

County (USNM 929-2)) and Jean-Alix Barrat (Agoult, NWA 2362). The reviewers, guest associate editor, and associate editor are thanked for their insightful feedback and suggestions. Candice Bedford is thanked for their help and guidance on statistical analysis. Nicola Potts is also thanked for their input and advice.

APPENDIX A. SUPPLEMENTARY MATERIAL

Supplementary data to this article can be found online at https://doi.org/10.1016/j.gca.2019.06.024.

REFERENCES

Alexander C. M. O. D., Bowden R., Fogel M. L., Howard K. T., Herd C. D. K. and Nittler L. R. (2012) The Provenances of Asteroids, and Their Contributions to the Volatile Inventories of the Terrestrial Planets. *Science* **337**, 721–723.

Barnes J. J., Franchi I. A., Anand M., Tartèse R., Starkey N. A., Koike M., Sano Y. and Russell S. S. (2013) Accurate and precise measurements of the D/H ratio and hydroxyl content in lunar apatites using NanoSIMS. *Chem. Geol.* **337–338**, 48–55.

Barnes J. J., Tartèse R., Anand M., McCubbin F. M., Neal C. R. and Franchi I. A. (2016) Early degassing of lunar urKREEP by crust-breaching impact(s). *Earth Planet. Sci. Lett.* **447**, 84–94.

Barnes J. J., Franchi I. A., McCubbin F. M. and Anand M. (2019) Multiple reservoirs of volatiles in the Moon revealed by the isotopic composition of chlorine in lunar basalts. *Geochim. Cosmochim. Acta* **266**, 144–162.

Barrat J.-A., Blichert-Toft J., Gillet P. and Keller F. (2000) The differentiation of eucrites: the role of in situ crystallization. *Meteorit. Planet. Sci.* **35**, 1087–1100.

Barrat J.-A. (2004) Determination of parental magmas of HED cumulates: The effects of interstitial melts. *Meteorit. Planet. Sci.* **39**, 1767–1779.

Barrat J.-A., Yamaguchi A., Greenwood R., Bohn M., Cotten J., Benoit M. and Franchi I. (2007) The Stannern trend eucrites: Contamination of main group eucritic magmas by crustal partial melts. *Geochim. Cosmochim. Acta* **71**, 4108–4124.

Barrat J. A., Yamaguchi A., Bunch T. E., Bohn M., Bollinger C. and Ceuleneer G. (2011) Possible fluid–rock interactions on differentiated asteroids recorded in eucritic meteorites. *Geochim. Cosmochim. Acta* **75**, 3839–3852.

Barrat J.-A., Yamaguchi A., Jambon A., Bollinger C. and Boudouma O. (2012) Low-Mg rock debris in howardites: Evidence for KREEPy lithologies on Vesta? *Geochim. Cosmochim. Acta* **99**, 193–205.

Barrett T. J., Barnes J. J., Tartèse R., Anand M., Franchi I. A., Greenwood R. C., Charlier B. L. A. and Grady M. M. (2016) The abundance and isotopic composition of water in eucrites. *Meteorit. Planet. Sci.* **51**, 1110–1124.

Bellucci J. J., Whitehouse M. J., John T., Nemchin A. A., Snape J. F., Bland P. A. and Benedix G. K. (2017) Halogen and Cl isotopic systematics in Martian phosphates: Implications for the Cl cycle and surface halogen reservoirs on Mars. *Earth Planet. Sci. Lett.* **458**, 192–202.

Boesenberg J. S. and Delaney J. S. (1997) A model composition of the basaltic achondrite planetoid. *Geochim. Cosmochim. Acta* **61**, 3205–3225.

Bogard D. D. and Garrison D. H. (2003) ^{39}Ar-^{40}Ar ages of eucrites and thermal history of asteroid 4 Vesta. *Meteorit. Planet. Sci.* **38**, 669–710.

Bonifacie M., Jendrzejewski N., Agrinier P., Humler E., Coleman M. and Javoy M. (2008) The chlorine isotope composition of Earth's mantle. *Science* **319**, 1518–1520.

Bottke W. F., Vokrouhlický D., Marchi S., Swindle T., Scott E. R. D., Weirich J. R. and Levison H. (2015) Dating the Moon-forming impact event with asteroidal meteorites. *Science* **348**, 321–323.

Bouvier L. C., Costa M. M., Connelly J. N., Jensen N. K., Wielandt D., Storey M., Nemchin A. A., Whitehouse M. J., Snape J. F., Bellucci J. J., Moynier F., Agranier A., Gueguen B., Schönbächler M. and Bizzarro M. (2018) Evidence for extremely rapid magma ocean crystallization and crust formation on Mars. *Nature* **558**, 586–589.

Boyce J. W., Tomlinson S. M., McCubbin F. M., Greenwood J. P. and Treiman A. H. (2014) The lunar apatite paradox. *Science* **344**, 400–402.

Boyce J. W., Treiman A. H., Guan Y., Ma C., Eiler J. M., Gross J., Greenwood J. P. and Stolper E. M. (2015) The chlorine isotope fingerprint of the lunar magma ocean. *Sci. Adv.* **1**.

Bridges J. C., Banks D. A., Smith M. and Grady M. M. (2004) Halite and stable chlorine isotopes in the Zag H3–6 breccia. *Meteorit. Planet. Sci.* **39**, 657–666.

Chen H., Savage P. S., Teng F.-Z., Helz R. T. and Moynier F. (2013) Zinc isotope fractionation during magmatic differentiation and the isotopic composition of the bulk Earth. *Earth Planet. Sci. Lett.* **369**, 34–42.

Dauphas N. and Pourmand A. (2011) Hf-W-Th evidence for rapid growth of Mars and its status as a planetary embryo. *Nature* **473**, 489–492.

Day J. M. D. and Moynier F. (2014) Evaporative fractionation of volatile stable isotopes and their bearing on the origin of the Moon. *Philos. Trans. Roy. Soc. A: Math. Phys. Eng. Sci.* **372**.

Day J. M. D., Moynier F., Meshik A. P., Pradivtseva O. V. and Petit D. R. (2017a) Evaporative fractionation of zinc during the first nuclear detonation. *Sci. Adv.* **3**.

Day J. M. D., Moynier F. and Shearer C. K. (2017b) Late-stage magmatic outgassing from a volatile-depleted Moon. *Proc. Natl. Acad. Sci.* **114**, 9547–9551.

De Sanctis M. C., Ammannito E., Capria M. T., Tosi F., Capaccioni F., Zambon F., Carraro F., Fonte S., Frigeri A., Jaumann R., Magni G., Marchi S., McCord T. B., McFadden L. A., McSween H. Y., Mittlefehldt D. W., Nathues A., Palomba E., Pieters C. M., Raymond C. A., Russell C. T., Toplis M. J. and Turrini D. (2012) Spectroscopic characterization of mineralogy and its diversity across vesta. *Science* **336**, 697–700.

Delaney J., O'neill C. and Prinz M. (1984) Phosphate minerals in eucrites. In *Lunar and Planetary Institute Science Conference Abstracts*, pp. 208–209.

Dhaliwal J. K., Day J. M. D. and Moynier F. (2017) Volatile element loss during planetary magma ocean phases. *Icarus*.

Eggenkamp H. G. M., Middelburg J. J. and Kreulen R. (1994) Preferential diffusion of ^{35}Cl relative to ^{37}Cl in sediments of Kau Bay, Halmahera, Indonesia. *Chem. Geol.* **116**, 317–325.

Eggenkamp H. G. M. and Coleman M. L. (2009) The effect of aqueous diffusion on the fractionation of chlorine and bromine stable isotopes. *Geochim. Cosmochim. Acta* **73**, 3539–3548.

Eggenkamp H. (2014) Theoretical and experimental fractionation studies of chloride and bromide isotopes. In *Springer*, pp. 75–93. Springer.

Fortin M.-A., Watson E. B. and Stern R. (2017) The isotope mass effect on chlorine diffusion in dacite melt, with implications for fractionation during bubble growth. *Earth Planet. Sci. Lett.* **480**, 15–24.

Goldoff B., Webster J. D. and Harlov D. E. (2012) Characterization of fluor-chlorapatites by electron probe microanalysis with a focus on time-dependent intensity variation of halogens. *Am. Mineral.* **97**, 1103–1115.

Greenwood R. C., Franchi I. A., Jambon A. and Buchanan P. C. (2005) Widespread magma oceans on asteroidal bodies in the early solar system. *Nature* **435**, 916–918.

Hsu W. and Crozaz G. (1996) Mineral chemistry and the petrogenesis of eucrites: I. Noncumulate eucrites. *Geochim. Cosmochim. Acta* **60**, 4571–4591.

Hu S., Lin Y., Zhang J., Hao J., Xing W., Zhang T., Yang W. and Changela H. (2019) Ancient geologic events on Mars revealed by zircons and apatites from the Martian regolith breccia NWA 7034. *Meteorit. Planet. Sci.* **54**, 850–879.

Hutchison R. (2004) Meteorites: A Petrologic, Chemical and Isotopic Synthesis. Cambridge University Press.

Kato C., Moynier F., Valdes M. C., Dhaliwal J. K. and Day J. M. D. (2015) Extensive volatile loss during formation and differentiation of the Moon. *Nat. Commun.* **6**, 7617.

Kato C. and Moynier F. (2017) Gallium isotopic evidence for extensive volatile loss from the Moon during its formation. *Sci. Adv.* **3**.

Kaufmann R., Long A., Bentley H. and Davis S. (1984) Natural chlorine isotope variations. *Nature* **309**, 338–340.

Lodders K., Fegley B. and Lodders F. (1998) The planetary scientist's companion. Oxford University Press on Demand.

Lodders K. (2003) Solar system abundances and condensation temperatures of the elements. *Astrophys. J.* **591**, 1220.

Magenheim A., Spivack A., Volpe C. and Ransom B. (1994) Precise determination of stable chlorine isotopic ratios in low-concentration natural samples. *Geochim. Cosmochim. Acta* **58**, 3117–3121.

Manzini M., Bouvier A.-S., Barnes J. D., Bonifacie M., Rose-Koga E. F., Ulmer P., Métrich N., Bardoux G., Williams J., Layne G. D., Straub S., Baumgartner L. P. and John T. (2017) SIMS chlorine isotope analyses in melt inclusions from arc settings. *Chem. Geol.* **449**, 112–122.

Mayne R., McSween H., McCoy T. and Gale A. (2009) Petrology of the unbrecciated eucrites. *Geochim. Cosmochim. Acta* **73**, 794–819.

McCord T. B., Adams J. B. and Johnson T. V. (1970) Asteroid Vesta: Spectral reflectivity and compositional implications. *Science* **168**, 1445–1447.

McCubbin F. M., Steele A., Nekvasil H., Schnieders A., Rose T., Fries M., Carpenter P. K. and Jolliff B. L. (2010) Detection of structurally bound hydroxyl in fluorapatite from Apollo Mare basalt 15058,128 using TOF-SIMS. *Am. Mineral.* **95**, 1141–1150.

McCubbin F. M., Hauri E. H., Elardo S. M., Vander Kaaden K. E., Wang J. and Shearer C. K. (2012) Hydrous melting of the martian mantle produced both depleted and enriched shergottites. *Geology* **40**, 683–686.

McCubbin F. M. and Jones R. H. (2015) Extraterrestrial apatite: planetary geochemistry to astrobiology. *Elements* **11**, 183–188.

McCubbin F. M., Vander Kaaden K. E., Tartèse R., Boyce J. W., Mikhail S., Whitson E. S., Bell A. S., Anand M., Franchi I. A., Wang J. and Hauri E. H. (2015) Experimental investigation of F, Cl, and OH partitioning between apatite and Fe-rich basaltic melt at 1.0–1.2 GPa and 950–1000 °C. *Am. Mineral.* **100**, 1790–1802.

McSween H. Y., Binzel R. P., De Sanctis M. C., Ammannito E., Prettyman T. H., Beck A. W., Reddy V., Le Corre L., Gaffey M. J., McCord T. B., Raymond C. A., Russell C. T. and the Dawn Science T. (2013) Dawn; the Vesta–HED connection; and the geologic context for eucrites, diogenites, and howardites. *Meteorit. Planet. Sci.* **48**, 2090–2104.

Misawa K., Yamaguchi A. and Kaiden H. (2005) U-Pb and ^{207}-Pb-^{206}Pb ages of zircons from basaltic eucrites: Implications for early basaltic volcanism on the eucrite parent body. *Geochim. Cosmochim. Acta* **69**, 5847–5861.

Mittlefehldt D. W. and Lindstrom M. M. (2003) Geochemistry of eucrites: Genesis of basaltic eucrites, and Hf and Ta as petrogenetic indicators for altered Antarctic eucrites. *Geochim. Cosmochim. Acta* **67**, 1911–1934.

Mittlefehldt D. W. (2015) Asteroid (4) Vesta: I. The howardite-eucrite-diogenite (HED) clan of meteorites. *Chem. Erde* **75**, 155–183.

Moynier F., Beck P., Jourdan F., Yin Q.-Z., Reimold U. and Koeberl C. (2009) Isotopic fractionation of zinc in tektites. *Earth Planet. Sci. Lett.* **277**, 482–489.

Moynier F. and Le Borgne M. (2015) High precision zinc isotopic measurements applied to mouse organs. *Journal of visualized experiments: JoVE*, e52479–e52479.

Moynier F., Vance D., Fujii T. and Savage P. (2017) The isotope geochemistry of zinc and copper. *Rev. Mineral. Geochem.* **82**, 543–600.

Newman S., Epstein S. and Stolper E. (1988) Water, carbon dioxide, and hydrogen isotopes in glasses from the ca. 1340 A. D. eruption of the Mono Craters, California: Constraints on degassing phenomena and initial volatile content. *J. Volcanol. Geoth. Res.* **35**, 75–96.

Paniello R. C., Moynier F., Beck P., Barrat J.-A., Podosek F. A. and Pichat S. (2012) Zinc isotopes in HEDs: Clues to the formation of 4-Vesta, and the unique composition of Pecora Escarpment 82502. *Geochim. Cosmochim. Acta* **86**, 76–87.

Pernet-Fisher J. F., Howarth G. H., Liu Y., Chen Y. and Taylor L. A. (2014) Estimating the lunar mantle water budget from phosphates: Complications associated with silicate-liquid-immiscibility. *Geochim. Cosmochim. Acta* **144**, 326–341.

Potts N. J., Tartèse R., Anand M., van Westrenen W., Griffiths A. A., Barrett T. J. and Franchi I. A. (2016) Characterization of mesostasis regions in lunar basalts: Understanding late-stage melt evolution and its influence on apatite formation. *Meteorit. Planet. Sci.* **51**, 1555–1575.

Potts N. J., Barnes J. J., Tartèse R., Franchi I. A. and Anand M. (2018) Chlorine isotopic compositions of apatite in Apollo 14 rocks: Evidence for widespread vapor-phase metasomatism on the lunar nearside ~4 billion years ago. *Geochim. Cosmochim. Acta* **230**, 46–59.

Pringle E. A. and Moynier F. (2017) Rubidium isotopic composition of the Earth, meteorites, and the Moon: Evidence for the origin of volatile loss during planetary accretion. *Earth Planet. Sci. Lett.* **473**, 62–70.

Pringle E. A., Moynier F., Beck P., Paniello R. and Hezel D. C. (2017) The origin of volatile element depletion in early solar system material: Clues from Zn isotopes in chondrules. *Earth Planet. Sci. Lett.* **468**, 62–71.

Robert F. (2006) Solar system deuterium/hydrogen ratio. *Meteorit. Early Solar Syst. II* **1**, 341–351.

Roszjar J., Metzler K., Bischoff A., Barrat J.-A., Geisler T., Greenwood R. C., Franchi I. A. and Klemme S. (2011) Thermal history of Northwest Africa 5073—A coarse-grained Stannern-trend eucrite containing cm-sized pyroxenes and large zircon grains. *Meteorit. Planet. Sci.* **46**, 1754–1773.

Roszjar J., John T. and Whitehouse M. J. (2015) Halogens from the early solar system – insights from meteoritic phosphates. *5th Misasa International Symposium*.

Sarafian A. R., Roden M. F. and Patiño-Douce A. E. (2013) The volatile content of Vesta: Clues from apatite in eucrites. *Meteorit. Planet. Sci.* **48**, 2135–2154.

Sarafian A. R., Nielsen S. G., Marschall H. R., McCubbin F. M. and Monteleone B. D. (2014) Early accretion of water in the inner solar system from a carbonaceous chondrite–like source. *Science* **346**, 623–626.

Sarafian A. R., Hauri E. H., McCubbin F. M., Lapen T. J., Berger E. L., Nielsen S. G., Marschall H. R., Gaetani G. A., Righter

K. and Sarafian E. () Early accretion of water and volatile elements to the inner Solar System: evidence from angrites. *Philos. Trans. Roy. Soc. A: Math. Phys. Eng. Sci.* **375**.

Sarafian A. R., John T., Roszjar J. and Whitehouse M. J. (2017b) Chlorine and hydrogen degassing in Vesta's magma ocean. *Earth Planet. Sci. Lett.* **459**, 311–319.

Sarafian A. R., Nielsen S. G., Marschall H. R., Gaetani G. A., Hauri E. H., Righter K. and Berger E. L. (2017c) Volatile concentrations and H-isotope composition of unequilibrated eucrites. *48th Lunar and Planetary Science Conference, Abstract #1436*.

Schauble E. A., Rossman G. R. and Taylor H. (2003) Theoretical estimates of equilibrium chlorine-isotope fractionations. *Geochim. Cosmochim. Acta* **67**, 3267–3281.

Schneck U. G., Boyce J. W., Treiman A. H., Eiler J. M., Guan Y. and Ma C. (2016) Testing the urKREEP-δ^{37}Cl hypothesis with eucrites. In *Lunar and Planetary Science Conference, Abstract #2978*, p. 2199.

Scott E. R. D., Greenwood R. C., Franchi I. A. and Sanders I. S. (2009) Oxygen isotopic constraints on the origin and parent bodies of eucrites, diogenites, and howardites. *Geochim. Cosmochim. Acta* **73**, 5835–5853.

Sharp Z. D., Barnes J. D., Brearley A. J., Chaussidon M., Fischer T. P. and Kamenetsky V. S. (2007) Chlorine isotope homogeneity of the mantle, crust and carbonaceous chondrites. *Nature* **446**, 1062–1065.

Sharp Z. D., Barnes J. D., Fischer T. P. and Halick M. (2010a) An experimental determination of chlorine isotope fractionation in acid systems and applications to volcanic fumaroles. *Geochim. Cosmochim. Acta* **74**, 264–273.

Sharp Z. D., Shearer C. K., McKeegan K. D., Barnes J. D. and Wang Y. Q. (2010b) The Chlorine Isotope Composition of the Moon and Implications for an Anhydrous Mantle. *Science* **329**, 1050–1053.

Sharp Z. D., McCubbin F. M. and Shearer C. K. (2013a) A hydrogen-based oxidation mechanism relevant to planetary formation. *Earth Planet. Sci. Lett.* **380**, 88–97.

Sharp Z. D., Mercer J. A., Jones R. H., Brearley A. J., Selverstone J., Bekker A. and Stachel T. (2013b) The chlorine isotope composition of chondrites and Earth. *Geochim. Cosmochim. Acta* **107**, 189–204.

Sharp Z. D., Williams J. T., Shearer C. K., Agee C. B. and McKeegan K. D. (2016) The chlorine isotope composition of Martian meteorites 2. Implications for the early solar system and the formation of Mars. *Meteorit. Planet. Sci.* **51**, 2111–2126.

Shearer C. K., Messenger S., Sharp Z. D., Burger P. V., Nguyen A. N. and McCubbin F. M. (2018) Distinct chlorine isotopic reservoirs on Mars.: Implications for character, extent and relative timing of crustal interaction with mantle-derived magmas, evolution of the martian atmosphere, and the building blocks of an early Mars. *Geochim. Cosmochim. Acta* **234**, 24–36.

Sossi P. A., Nebel O., O'Neill H. S. C. and Moynier F. (2018) Progressive accretion of Earth's moderately volatile elements revealed by Zn isotopes. *Chem. Geol.* **477**.

Stephant A., Hervig R., Bose M. and Wadhwa M. (2016) D/H ratios and water contents in eucrite minerals: Implications for the source and abundance of water on Vesta. *Annual meeting of the Meteoritical Society*.

Stock M. J., Humphreys M., Smith V. C., Johnson R. D. and Pyle D. M. (2015) New constraints on electron-beam induced halogen migration in apatite. *Am. Mineral.* **100**, 281–293.

Stolper E. (1977) Experimental petrology of eucritic meteorites. *Geochim. Cosmochim. Acta* **41**, 587–611.

Stormer J. C., Pierson M. L. and Tacker R. C. (1993) Variation of F and Cl X-ray intensity due to anisotropic diffusion in apatite. *Am. Mineral.* **78**, 641–648.

Takeda H. and Graham A. (1991) Degree of equilibration of eucritic pyroxenes and thermal metamorphism of the earliest planetary crust. *Meteoritics* **26**, 129–134.

Tartèse R., Anand M., Joy K. H. and Franchi I. A. (2014) H and Cl isotope systematics of apatite in brecciated lunar meteorites Northwest Africa 4472, Northwest Africa 773, Sayh al Uhaymir 169, and Kalahari 009. *Meteorit. Planet. Sci.* **49**, 2266–2289.

Toplis M. J., Mizzon H., Monnereau M., Forni O., McSween H. Y., Mittlefehldt D. W., McCoy T. J., Prettyman T. H., De Sanctis M. C., Raymond C. A. and Russell C. T. (2013) Chondritic models of 4 Vesta: Implications for geochemical and geophysical properties. *Meteorit. Planet. Sci.* **48**, 2300–2315.

Touboul M., Sprung P., Aciego S. M., Bourdon B. and Kleine T. (2015) Hf–W chronology of the eucrite parent body. *Geochim. Cosmochim. Acta* **156**, 106–121.

Treiman A. H. (1997) The parent magmas of the cumulate eucrites: A mass balance approach. *Meteorit. Planet. Sci.* **32**, 217–230.

Ustunisik G., Nekvasil H., Lindsley D. H. and McCubbin F. M. (2015) Degassing pathways of Cl-, F-, H-, and S-bearing magmas near the lunar surface: Implications for the composition and Cl isotopic values of lunar apatite. *Am. Mineral.* **100**, 1717–1727.

Wales E. and Boyce J. (2016) A terrestrial perspective on the record of lunar volatiles as recorded by apatite. *Lunar and Planetary Science Conference, Abstract #2181*.

Wang K., Moynier F., Dauphas N., Barrat J.-A., Craddock P. and Sio C. K. (2012) Iron isotope fractionation in planetary crusts. *Geochim. Cosmochim. Acta* **89**, 31–45.

Warren P. H. and Jerde E. A. (1987) Composition and origin of Nuevo Laredo trend eucrites. *Geochim. Cosmochim. Acta* **51**, 713–725.

Warren P. H., Rubin A. E., Isa J., Gessler N., Ahn I. and Choi B.-G. (2014) Northwest Africa 5738: Multistage fluid-driven secondary alteration in an extraordinarily evolved eucrite. *Geochim. Cosmochim. Acta* **141**, 199–227.

Weyer S. and Ionov D. A. (2007) Partial melting and melt percolation in the mantle: The message from Fe isotopes. *Earth Planet. Sci. Lett.* **259**, 119–133.

Wiechert U. H., Halliday A. N., Palme H. and Rumble D. (2004) Oxygen isotope evidence for rapid mixing of the HED meteorite parent body. *Earth Planet. Sci. Lett.* **221**, 373–382.

Williams J. T., Shearer C. K., Sharp Z. D., Burger P. V., McCubbin F. M., Santos A. R., Agee C. B. and McKeegan K. D. (2016) The chlorine isotopic composition of Martian meteorites 1: Chlorine isotope composition of Martian mantle and crustal reservoirs and their interactions. *Meteorit. Planet. Sci.* **51**, 2092–2110.

Yamaguchi A., Taylor G. J. and Keil K. (1996) Global Crustal Metamorphism of the Eucrite Parent Body. *Icarus* **124**, 97–112.

Yamaguchi A., Barrat J. A., Greenwood R. C., Shirai N., Okamoto C., Setoyanagi T., Ebihara M., Franchi I. A. and Bohn M. (2009) Crustal partial melting on Vesta: Evidence from highly metamorphosed eucrites. *Geochim. Cosmochim. Acta* **73**, 7162–7182.

Zhou Q., Yin Q.-Z., Young E. D., Li X.-H., Wu F.-Y., Li Q.-L., Liu Y. and Tang G.-Q. (2013) SIMS Pb–Pb and U-Pb age determination of eucrite zircons at <5μm scale and the first 50Ma of the thermal history of Vesta. *Geochim. Cosmochim. Acta* **110**, 152–175.

Associate editor: Geoffrey Hamilton Howarth